International Journal of Heat and Mass Transfer 204 (2023) 123855

Contents lists available at ScienceDirect

International Journal of Heat and Mass Transfer

journal homepage: www.elsevier.com/locate/hmt

Experimental study of flow boiling pressure drop and heat transfer of R1233zd(E) at moderate and high saturation temperatures

Michał Pysz*, Stanisław Głuch, Dariusz Mikielewicz

Faculty of Mechanical Engineering and Ship Technology, Gdańsk University of Technology, ul. Narutowicza 11/12, Gdańsk 80-233, Poland

ARTICLE INFO

Article history:
Received 14 July 2022
Revised 18 October 2022
Accepted 8 January 2023
Available online 15 January 2023

Keywords:
Thermodynamic critical point
Flow boiling
Heat transfer coefficient
Pressure drop
Modeling
Energy efficiency

ABSTRACT

The paper presents the results of experimental study of flow boiling of R1233zd(E) in minichannel at moderate and high saturation temperatures. The heat transfer coefficient and pressure drop were measured for flow boiling in a stainless steel tube with 2 mm inside diameter and a length of 300 mm. Experiment has been conducted for saturation temperatures ranging from 83 to 145 °C which corresponds to values of reduced pressures ranging from 0.2 to 0.7. Three different heat fluxes were analyzed, namely 20, 30 and 45 kW/m^2 and mass velocities ranged from 200 to 1000 kg/m^{2}s. The effects of reduced pressure, mass velocity, heat flux, vapor quality and flow regime were analyzed. At low reduced pressures ($p_r \leq 0.3$) heat transfer is driven by convective boiling mostly with nucleate boiling having effect only in the case of low mass velocities. Heat transfer in this case increases with mass velocity and vapor quality and is independent of heat flux. For reduced pressures of 0.4 and 0.5 both nucleate and convective boiling are present, however the nucleate boiling starts to be more dominant here, especially for low mass velocities and high heat fluxes. For low mass velocities and/or higher heat fluxes the heat transfer decrease or is independent of vapor quality, whereas for higher mass fluxes and/or lower heat fluxes it is initially independent of vapor quality and starts to increase close to the transition from intermittent to annular flow. At the range of high reduced pressures ($p_r \geq 0.6$) nucleate boiling is the dominant heat transfer mechanism. Experimental results were compared with some well-known two-phase flow correlations.

1. Introduction

Recently there is observed an increased interest in the development of new heat transfer installations where either flow boiling or flow condensation are employed under conditions close to the thermodynamic critical point. For example, mentioned here can be the organic Rankine cycle (ORC) installations as well as high temperature heat pumps (HTHP) which are very attractive options for example in recovery of heat from industrial processes or waste heat. In these applications either new fluids are implemented or the known ones are used under conditions reaching the thermodynamic critical point. Prediction of pressure drop and heat transfer under such conditions can usually be made using empirical methods using models developed for specific fluids, however, these conditions of operation have scarcely been confirmed by experiments. Moreover, the methods developed for single fluids or a restricted number of fluids suffer from not being general and cannot be applicable to a variety of fluids. Lack of experimental evidence of pressure drop and heat transfer characteristics at moderated and high saturation pressures come from the fact that hitherto applications regarded mainly refrigeration applications, i.e. small values of reduced pressures. Reduced pressure is defined as a ratio of saturation pressure of the actual experiment to the value of pressure corresponding to the thermodynamic critical point. Literature review shows a gap in knowledge on flow boiling of low boiling point fluids at high saturation temperatures (above 120 °C) for medium/high values of reduced pressures (0.5–0.9).

In the vicinity of the thermodynamic critical point the properties of both liquid and vapor phases change dramatically, especially for the reduced pressures higher than 0.8 [1], the changes are summarized in Fig. 1 which was developed based on the data from EES software [2]. Additionally, due to almost non-existent surface tension, the flow structures present in flow boiling at moderate and high saturation pressures are different than those found at low values of reduced pressure.

Most of the existent experimental data on flow boiling near the thermodynamic critical point was conducted for horizontal channels. Very few works deal with vertical upflow. Notable for that topic is an excellent review recently published by Marchetto et al. [1]. The main conclusion from that study is that flow patterns

* Corresponding author.
E-mail address: michal.pysz@pg.edu.pl (M. Pysz).

https://doi.org/10.1016/j.ijheatmasstransfer.2023.123855

Nomenclature

C_p	specific heat
d	diameter
f	friction factor
G	mass velocity
h	enthalpy
h_{lv}	latent heat of vaporization
l	length
$\dot{m}$	mass flow
MAE	mean absolute error
p	pressure
$\dot{q}$	heat flux
$\dot{q}_v$	heat generation
r	radius
T	temperature
x	vapor quality

Greek symbols

α	heat transfer coefficient
δ	uncertainty
λ	thermal conductivity
ρ	density
σ	surface tension

Subscripts

h	hydraulic
in	inner
l	liquid state
pH	preheater
r	reduced conditions
sat	saturation
ss	stainless steel
sub	sublimation
test	test section
v	vapor state

for flow boiling heat transfer at moderate and high reduced pressures are not consistent. Authors divided them into three categories, namely of no influence, or decreasing and increasing trends. In the group of experimental results indicating increasing distributions which are mostly found for reduced pressures $p_r < 0.5$, the researchers highlighted the common presence of U-shaped distributions of heat transfer. In such specific cases, the heat transfer coefficient initially decreases which is associated with the nucleation process, and then starts to increase creating distributions which remind the letter 'u'. The latter increase stems from the suppression of nucleation process with simultaneous development of convective boiling process. Fig. 2 presents typical qualitative distributions of U-shaped type for different mass velocities.

Belyaev et al. [3] conducted experimental study of vertical upflow boiling heat transfer of R113 and RC318 in channels with diameters of 1.36 and 0.95 mm, respectively. Saturation temperature was examined in the range from 30 to 180 °C. Authors concluded that for values of reduced pressures higher than p_r=0.4 the heat transfer trends resemble the ones for conventional minichannels despite small diameter of test sections. Mawatari and Mori [4] also studied flow boiling in vertically positioned tube. The main subject of their study was related to post critical heat flux data. Investigators highlighted two different post-CHF heat transfer trends which were dependent on mass fluxes.

Charnay et al. [5–8] investigated flow boiling of R245fa in a horizontal tube of 3 mm inside diameter. The study was performed for saturation temperatures in the range from 60 to 120 °C. The major finding of that work was that with increase in saturation temperature the importance of nucleate boiling increases. That is a significant novelty in understanding the flow structures at higher reduced pressures in flow boiling. Dominance of nucleate boiling at high reduced pressures was also confirmed by many different works made for horizontal channels [9–12]. It is apparent that nucleate boiling is of increasing dominance in heat transfer and flow structures with increasing reduced pressures. Billiet et al. [9] tested R245fa in a 3 mm inside diameter horizontal channel for various saturation temperatures ranging from 40 to 125 °C. For low saturation temperature, the heat transfer coefficient increased with mass velocity and vapor quality, whereas for higher values of saturation temperature opposite trends were found. Convective boiling or both convective and nucleate boiling were found for lower reduced pressures. Lillo et al. [13] investigated flow boiling of R448A and R404A for reduced pressures lower than 0.5. They observed that for low mass velocities the heat transfer was dominated by nucle-

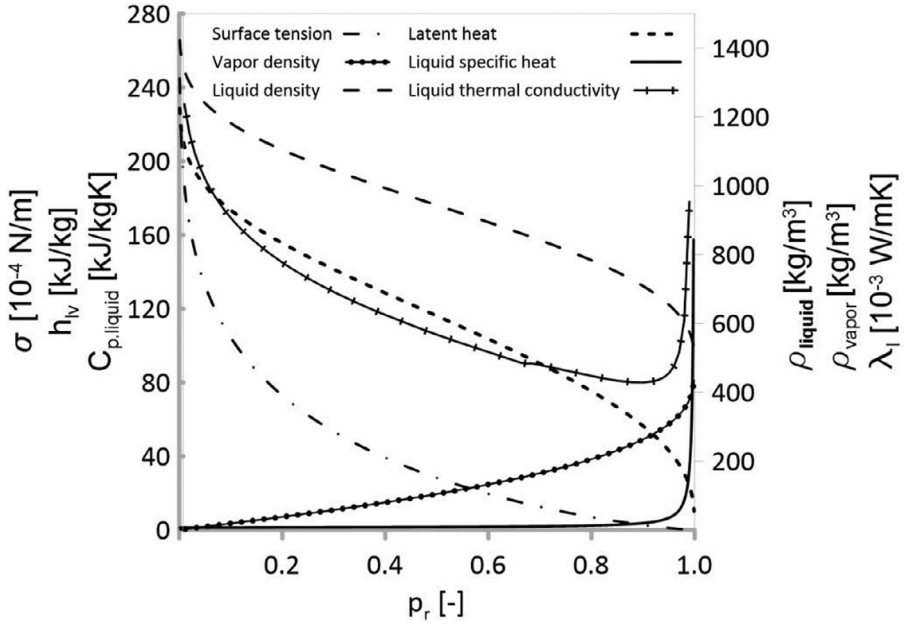

Fig. 1. Thermophysical properties of R1233zd(E) in function of reduced pressure, extracted from EES database [2].

Table 1
Overview of studies concerning heat transfer and pressure drop in the area of high reduced pressures and/or high saturation temperatures.

Authors	Fluid (p_r)	Shape of channel/orientation	D_h [mm]	$\dot{q}$ [kW/m^2]	G [kg/m^{2}s]
Belyaev et al. [3]	R113 (0.16–0.68); RC318 (0.69–0.9)	Cylindrical / vertical upflow	0.95–1.36	50.6–907	700–4830
Mawatari and Mori [4]	R134a (0.92–0.99); R22 (0.96–0.99)	Cylindrical / vertical upflow	4.4	9–48	400–1000
Charnay et al. [5–8]	R245fa (0.13–0.53)	Cylindrical / horizontal	3	10–50	300–1000
Billiet et al. [9]	R245fa (0.07–0.58)	Cylindrical / horizontal	3	10.9–54	100–1000
Grauso et al. [10]	R410A (0.19–0.52) CO_2 (0.57)	Cylindrical / horizontal	6	5–21.4	149–526
Zhang et al. [11]	R134a (0.62–0.81)	Cylindrical / horizontal	10.3	20–50	300–600
del Col [12]	R22 (0.27); R125 (0.39); R134a (0.19–0.29); R410A (0.49–0.50)	Cylindrical / horizontal	8	9–52.5	200–400
Lillo et al. [13]	R448A(0.27–0.46); R404A(0.33–0.54)	Cylindrical / horizontal	6	10–40	150–600
Guo et al. [14]	R134a (0.10–0.88) R245fa (0.11–0.31)	Cylindrical / horizontal	10	6–24	100–318

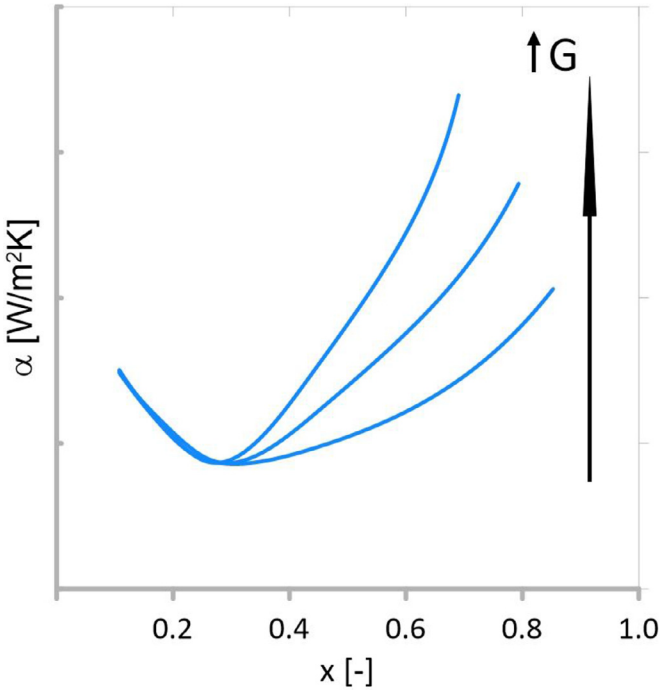

Fig. 2. U-shaped heat transfer trends for different mass velocities.

ate boiling, however for higher mass velocities ($G > 400$ kg/m^{2}s) the convective boiling was seen to be more dominant. Similarly, Guo et al. [14] noticed increase in heat transfer coefficient with vapor quality of R134a which suggests dominance of convective boiling. Such a trend was seen despite high values of reduced pressure reached during this study (0.1–0.88). The details of all presented above studies are summarized in Table 1.

The objective of the present paper is to accomplish a study of a very perspective new thermodynamic fluid R1233zd(E) at moderate and high saturation temperatures, which will confirm the general findings gathered to date. Both, pressure drop and heat transfer are studied. As a result the available database of pressure drop and heat transfer data will be increased.

2. Experimental setup

The experiment was carried out in order to measure the heat transfer and pressure drop of R-1233zd(E) during flow boiling in a vertical stainless steel tube of 2 mm inside diameter and 300 mm length. Saturation temperature varied in the range from 83 to 145 °C, which corresponded to reduced pressure variation from 0.2 to 0.7. Heat flux in the experiment varied between 15 and 45 kW/m^2 whereas mass velocities were examined in the range 200–1000 kg/m^{2}s, respectively. Table 2 presents values of the thermophysical properties of R1233zd(e) at the values of reduced pressure values considered in the tests [2].

Fig. 3 presents a schematic of experimental facility. It consists of two loops, that is the test fluid (working fluid) and oil loop. Refrigerant is circulated in the loop by the diaphragm pump. Its flowrate is measured using the Coriolis-type flowmeter. Next in the loop are found the microvalve, preheater, test section and then the test fluid goes directly to the condenser either through the by-pass or visualization section. Oil is used as a cooling fluid in the condenser. In order to maintain stable conditions at the inlet to the working fluid pump, the oil loop was equipped with a tank and a pump which assured high mass flow rates with small temperature difference between oil at the inlet and the outlet of condenser. Stable temperature of oil is assured thanks to the oversized tank cooled by network water.

The mass flow rate in the test section is controlled in three different ways: by rotational velocity of the pump, by the by-pass needle valve, or by the needle valve placed before the preheater. The saturation pressure in the system is sustained with the aid of the bladder accumulator which is filled with nitrogen on one side and the liquid working fluid on the other side. Additionally, accumulator serves as a flow and pressure stabilizer for the pump. A three meters long spirally formed preheater with inside diameter of 4.57 mm is preparing the required parameters for the test section, usually to feature the saturated conditions at inlet or in some cases initially evaporated. Preheater is used to control the vapor quality at the test section inlet. Preheater and test section are heated by the Joule effect using two separate DC voltage suppliers. Two pressure transducers and two K-type thermocouples are installed at the inlet and outlet of the test section. Eighteen K-type thermocouples are soldered to the wall of test section (respectively nine at the bottom and nine at the top). The details of section are presented in Fig. 3.

All of the thermocouples were calibrated at 3 different temperature points at certified laboratory. Preheater and test section are electrically insulated by PEEK separators. 3D model of the test section is presented in Fig. 4.

Visual test section consists of borosilicate glass tube with inside diameter of 3 mm and high speed camera. Visualization test section is presented in Fig. 5. Vapor exiting the test section is condensed and subcooled in a plate heat exchanger.

Data acquisition is made with a use of National Instruments NI PXIe-1071 (DAQ) connected to PC. National Instruments LabView software is used for this purpose with self-written code.

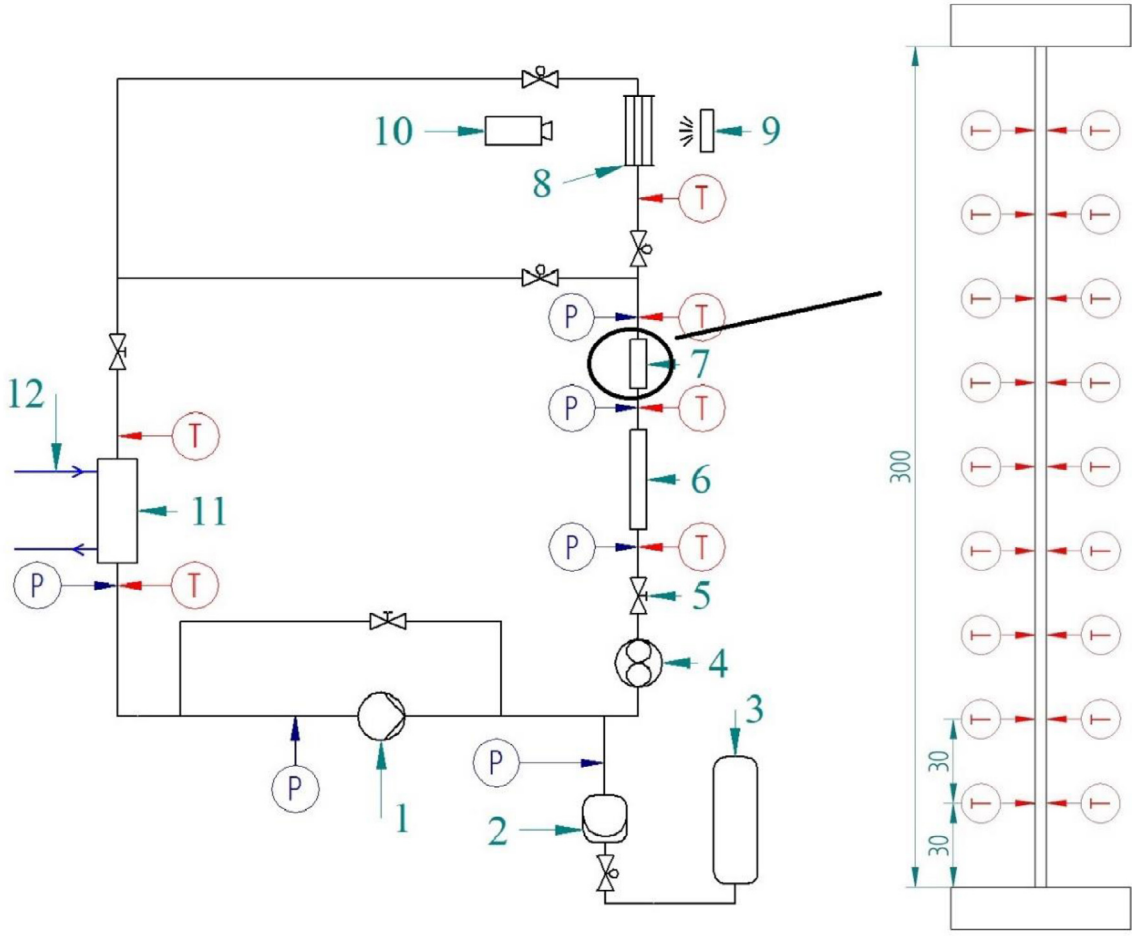

Fig. 3. Experimental facility schematic: 1 – diaphragm pump, 2 – bladder hydro-accumulator, 3 – pressurized nitrogen tank, 4 – Coriolis flowmeter, 5 – control valve, 6 – preheater, 7 – heat transfer test section, 8 – visualization test section, 9 – led light source, 10 – fast camera, 11 – condenser, 12 – oil loop.

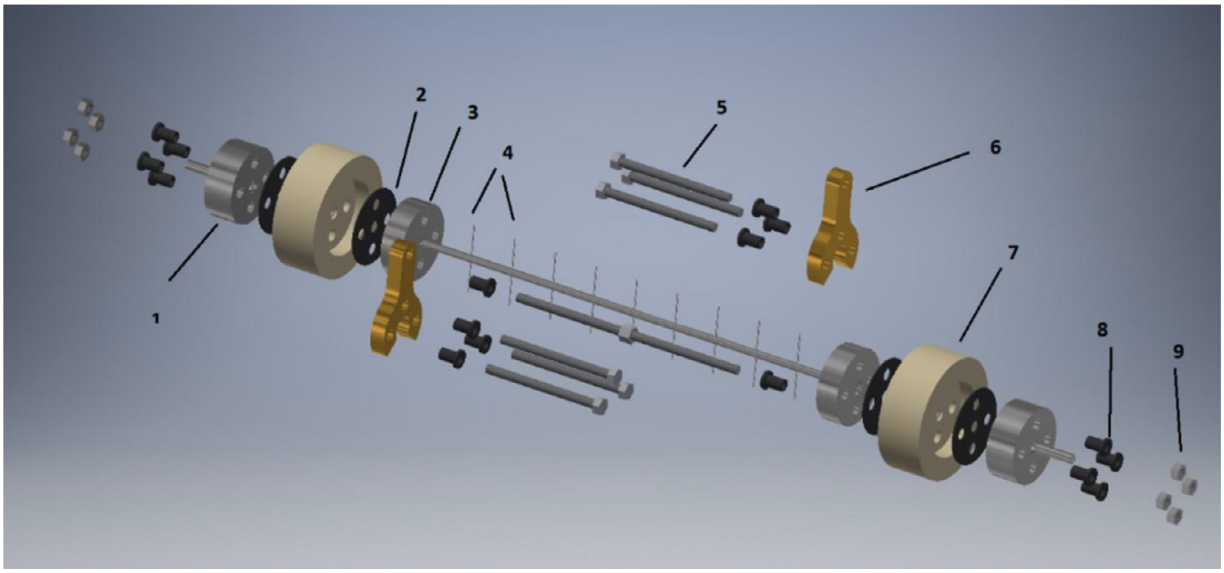

Fig. 4. 3D model of heat transfer test Section. 1 – fastening flange, 2 – Teflon seal, 3 – stainless-steel test section, 4- soldered thermocouples, 5 – screws, 6 – DC current connectors, 7 – PEEK electrical insulators, 8 – Teflon screw electrical insulators, 9 – nuts.

Table 2
Properties of R1233zd(E) at different reduced pressures used in experiment.

Reduced pressure [-]	Saturation temperature [C]	Pressure [bar]	Liquid specific heat [kJ/kg]	Heat of vaporization [kJ/kg]
0.2	83.41	7.14	1.35	155.57
0.3	101.26	10.71	1.41	141.38
0.4	115.07	14.28	1.49	128.55
0.5	126.48	17.85	1.58	116.15
0.6	136.27	21.43	1.72	103.59
0.7	144.85	24.99	1.94	90.25

Fig. 5. Visualization test section – borosilicate glass tube, d_{in} = 3 mm, l = 100 mm.

3. Data processing and reduction

Heat transfer coefficient and pressure drop of R1233zd(E) are measured during experiment.

The root-sum-square (RSS) method [15] is used for error propagation, which reads:

$$\delta q = \sqrt{\left(\frac{\partial q}{\partial x}\delta x\right)^2 + .. + \left(\frac{\partial q}{\partial z}\delta z\right)^2} \quad (1)$$

where q is the experimental result calculated based on other variables (x, ..., z) which are measured with known uncertainty δ. Examples of obtained uncertainty for the mean heat transfer coefficient are presented on Figs. 6 and 7:

The uncertainty of the heat transfer coefficient varied from few percent for post-dryout data to around 20% for the highest values of heat transfer coefficient due to small temperature difference between fluid and wall. Table 3 presents the experimental details with maximum values of calculated uncertainty.

Tests are carried out by monitoring mass flux and calculated values of vapor quality and saturation temperature. Data is recorded when certain conditions are satisfied in a time of 10 min, namely the deviation of mass flux lower than 1.5% of current value, the deviation of saturation temperature not higher than 0.5 °C and vapor quality deviation not higher than 1%.

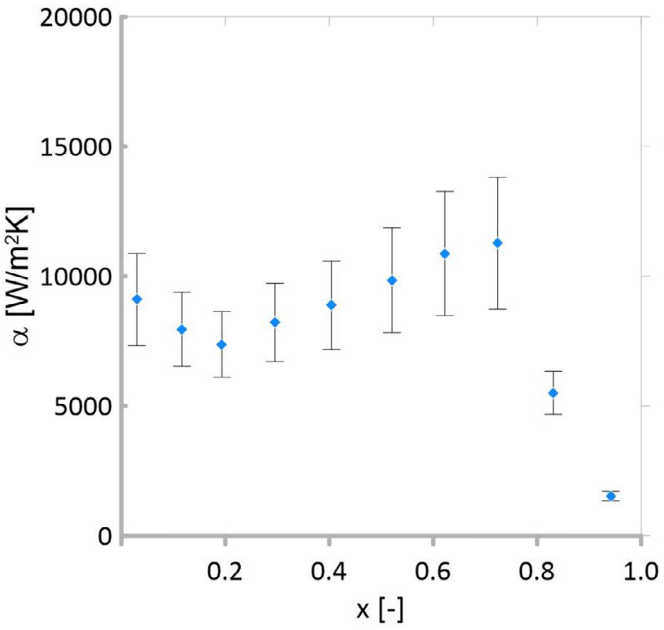

Fig. 6. The heat transfer coefficient in a function of vapor quality with calculated uncertainty – reduced pressure 0.4, G = 600 kg/m²s and q = 20 kW/m².

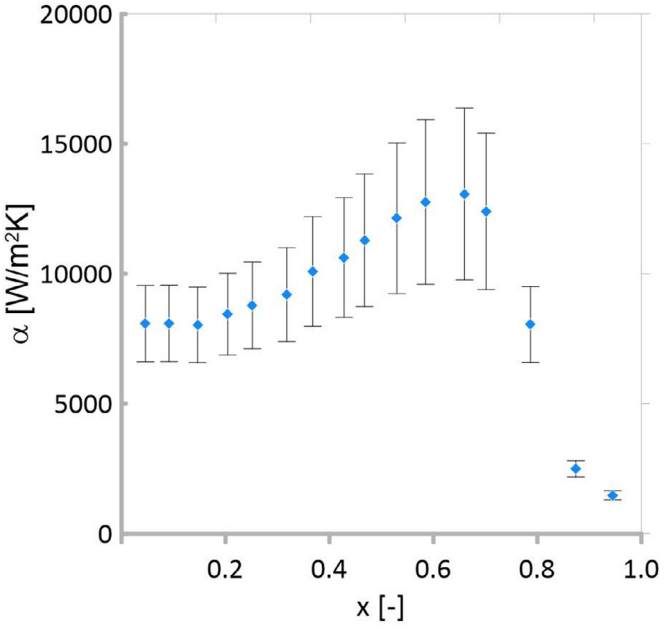

Fig. 7. The heat transfer coefficient in a function of vapor quality with calculated uncertainty – reduced ressure 0.4, G = 800 kg/m²s and q = 20 kW/m².

Table 3
Range of the experimental parameters in the study.

Parameters	Values	Maximum uncertainty
d (mm)	2.0	± 0.05
l (mm)	300	± 0.1
G (kg/m^{2}s)	400–1000	± 6.5%
$\dot{q}_{preheater}$ (kW/m^2)	0.1–50.0	± 4.5%
$\dot{q}_{test\ section}$ (kW/m^2)	20.0–45.0	± 10.2%
T_{sat} (°C)	83–145	± 0.5
P_{sat} (kPa):	714–1430	± 14.0

Enthalpy at the inlet of test section is calculated from the energy balance of the preheater:

$$h_1 = h_0 + \frac{\dot{Q}_{ph}}{\dot{m}} \tag{2}$$

where: h_0 is enthalpy at the inlet of preheater, calculated on the basis of temperature and pressure measurements, Q_{ph} is power output delivered to the preheater and m is the mass flow.

The vapor quality at position y of the test section is calculated with the local enthalpy calculations:

$$x_y = \frac{h_1 + \frac{\dot{Q}_{test}}{\dot{m}} \frac{l_y}{l_{test}} - h_{1,\ sat}}{h_{lv}} \tag{3}$$

where: x_y is vapor quality at the position y of the test section, h_1 is enthalpy at the inlet of test section calculated on the basis of temperature and pressure measurements, Q_{test} is power output delivered to test section, l_y is the position of the measurement point and l_{test} is the length of test section, $h_{1saturated}$ is the saturated liquid enthalpy at the inlet of test section and h_{lv} is latent heat of vaporization calculated for saturation temperature.

There are two cases possible during experiment, i.e. the one in which subcooled liquid enters the heat transfer test section and the second one in which the liquid-vapor mixture featuring some quality enters the test section.

In the first case in order to deduce the saturation temperature the single phase pressure drop at the beginning of the test section has to be calculated:

$$\Delta P_l = \frac{2 \cdot G^2 \cdot f_l \cdot l_{sub}}{\rho_l \cdot d_{in}} \tag{4}$$

where G denotes ~~a~~ mass velocity, l_{sub} is the subcooled length, f_l is friction factor calculated on the basis of Blasius correlation, ρ_l is a single phase density and d_{in} is inside diameter of test section.

Calculation of subcooled length is based on energy balance:

$$l_{sub} = \frac{\dot{m} \cdot c_p}{\dot{q}_{test} \cdot \pi \cdot d_{in}} \cdot (T_{sat} - T_1) \tag{5}$$

where q_{test} is heat flux generated in a tube by Joule effect.

Saturation temperature is deduced with the use of EES software on the basis of saturation pressure:

$$p_{sat.test} = p_{test.in} - \Delta p_l \tag{6}$$

Taking into account the saturation pressure from Eq. (6) the saturation temperature at position y for the first experimental case is calculated using EES software:

$$T_{sat.y} = T_{sat}(p_{sat.y}) \tag{7}$$

where saturation pressure is calculated from the following equation:

$$p_{sat.y} = p_{sat.test} - (\Delta p_{total} - \Delta p_l) \cdot \left(\frac{l_y - l_{sub}}{l_{test} - l_{sub}} \right) \tag{8}$$

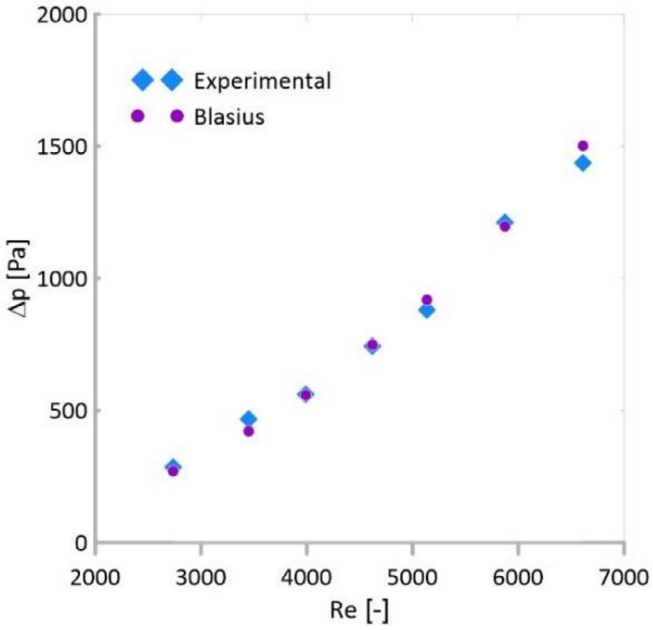

Fig. 8. Comparison of the experimental single-phase pressure drop with values obtained due Blasius [17].

In the second experimental case, where saturated two-phase fluid enters test section, the saturation pressure is calculated with the following equation:

$$p_{sat.y} = p_{sat.test.in} - (\Delta p_{total}) \cdot \left(\frac{l_y}{l_{test}} \right) \tag{9}$$

Temperature at the inner wall at position y (first thermocouple) is deduced from Eq. (10) which was derived based on the assumption of uniform heat generation in the channel.

$$T_{wall.in.y1} = T_{wall.out.y1} + \frac{\dot{q}_V \left(r_{outer}^2 - r_{inner}^2 \right)}{4 \cdot \lambda_{SS}} - \frac{\dot{q}_V \cdot r_{outer}^2}{2 \cdot \lambda_{SS}} \cdot \ln \left(\frac{r_{outer}}{r_{inner}} \right) \tag{10}$$

where $T_{wall.out.y1}$ is the temperature measured at position y, q_v is the volumetric heat generation, r_{outer} is the radius of outer wall, r_{inner} is the radius of inside wall and λ_{SS} is heat conductivity of the tube wall. Temperature inside the tube wall is calculated as average from both thermocouples located at position y:

$$T_{wall.in.y} = \frac{T_{wall.in.y1} + T_{wall.in.y2}}{2} \tag{11}$$

Finally the heat transfer coefficient at position y is calculated with Eq. (12):

$$\alpha_y = \frac{\dot{q}_{test}}{T_{wall.in.y} - T_{sat.y}} \tag{12}$$

4. Single-phase flow tests

Validation of experimental facility has been performed with the use of single-phase flow tests. Energy balance of the test section and the preheater showed that overall mean heat lost to the surroundings is equal to 8% and 12%, respectively. The heat transfer coefficient measurements were compared with the well-established correlation by Gnielinsky [16]. The pressure drop was compared with Blasius correlation [17]. The results of the comparison are presented in Figs. 8 and 9. The results achieved during tests were in good accuracy with models. Heat transfer coefficient was predicted with mean absolute percentage error of 6.79% by Gnielinsky correlation.

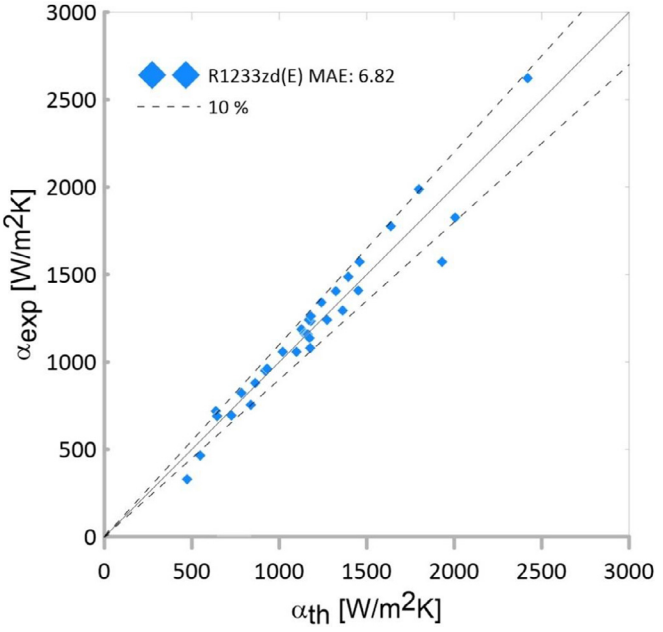

Fig. 9. Comparison of the single-phase test results α_{exp} with α_{th} obtained using the Gnielinski correlation [16].

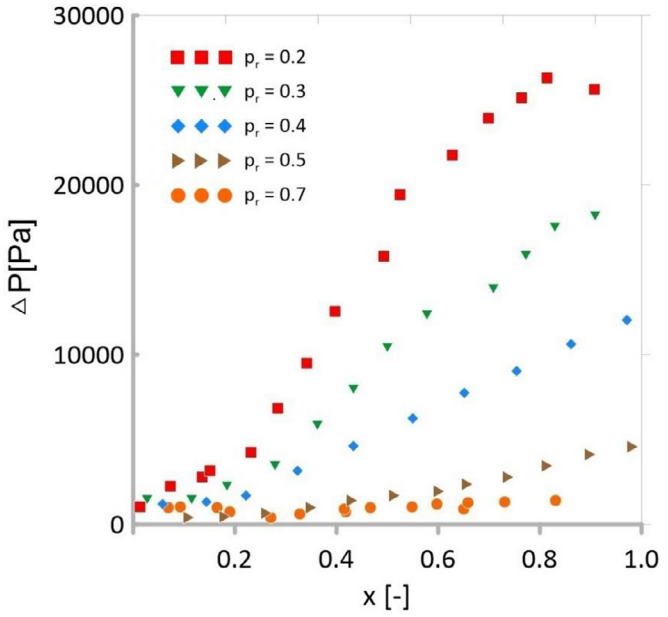

Fig. 10. Pressure drop in a function of vapor quality for different reduced pressures, mass velocity $G = 600$ kg/m^{2}s and heat flux $q = 20$ kW/m^2.

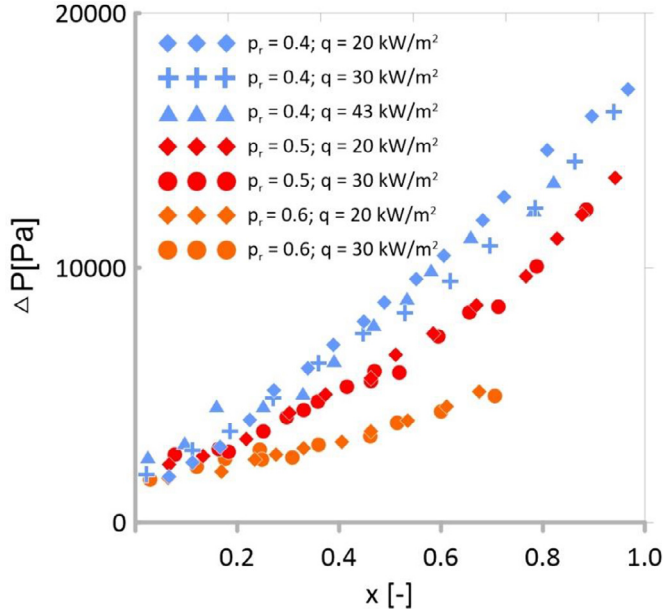

Fig. 11. Pressure drop in a function of vapor quality for different reduced pressures, different heat fluxes, and mass velocity $G = 800$ kg/m^{2}s.

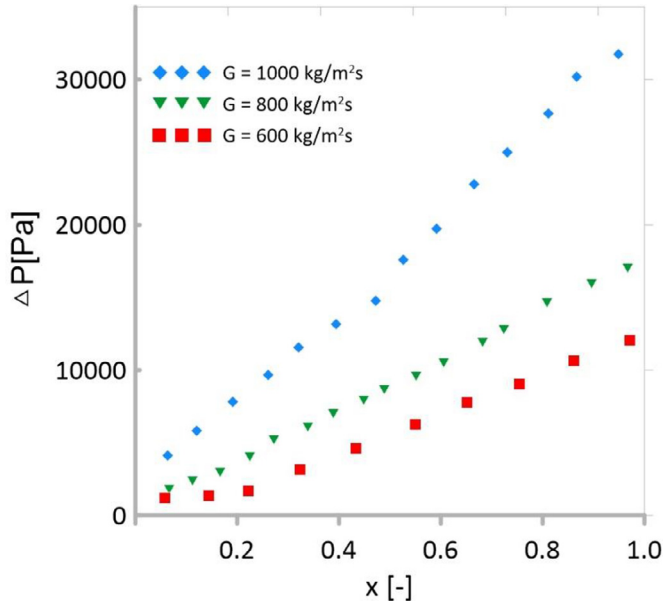

Fig. 12. Pressure drop in a function of vapor quality for different mass velocities, reduced pressure p_r=0.4, and heat flux $q = 20$ kW/m^2.

5. Results

Experiment has been conducted for saturation temperatures ranging from 83 to 145 °C which corresponds to values of reduced pressures from 0.2 to 0.7. Three different heat fluxes were analyzed, namely $q = 20$, 30 and 45 kW/m^2 whereas mass velocities ranged from 200 to 1000 kg/m^{2}s. The effects of reduced pressure, mass velocity, heat flux, vapor quality and flow regime were analyzed.

6. Pressure drop

Figs. 10–12 presents the pressure drop in function of vapor quality for various operating conditions. Fig. 10 shows the influence of reduced pressure on pressure drop for mass velocity, G equal to 600 kg/m^{2}s and heat flux equal to 20 kW/m^2. The higher are the values of reduced pressure the smaller the encountered pressure drop. Close to the thermodynamic critical point the liquid surface tension decreases which leads to smaller values of friction factor. Additionally the difference between phase velocities decrease which leads to smaller friction between the phases and in the same way to smaller pressure drop. Influence of heat flux on pressure drop is shown in Fig. 11. It can be noted that there is a negligible effect of applied heat flux on pressure drop. Some effect is present only at lower values of reduced pressure. In Fig. 12 presented is the relation of pressure drop to mass velocity at a constant value of reduced pressure, p_r=0.4, and a value of heat flux equal 20 kW/m^2. A typical dependence is obtained, that is the pressure drop increases with increasing mass velocity.

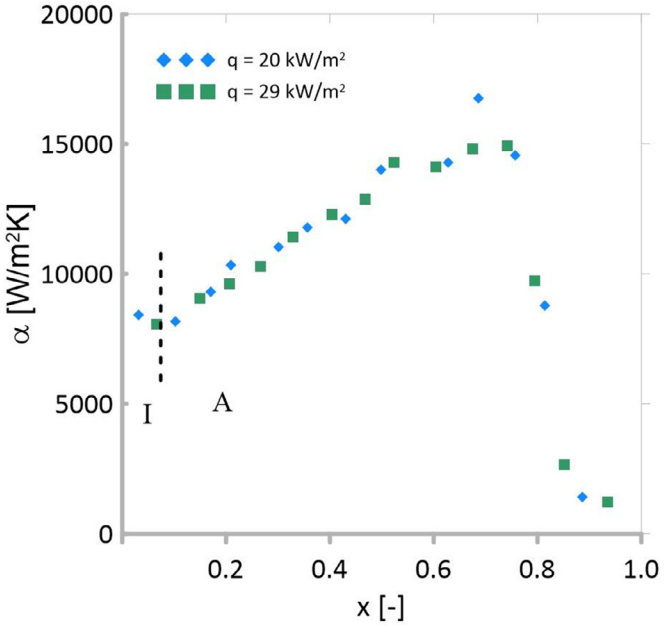

Fig. 13. Heat transfer coefficient in a function of vapor quality for different heat fluxes, reduced pressure p_r=0.2 and mass velocity G = 800 kg/m^{2}s (I – intermittent flow; A – annular flow).

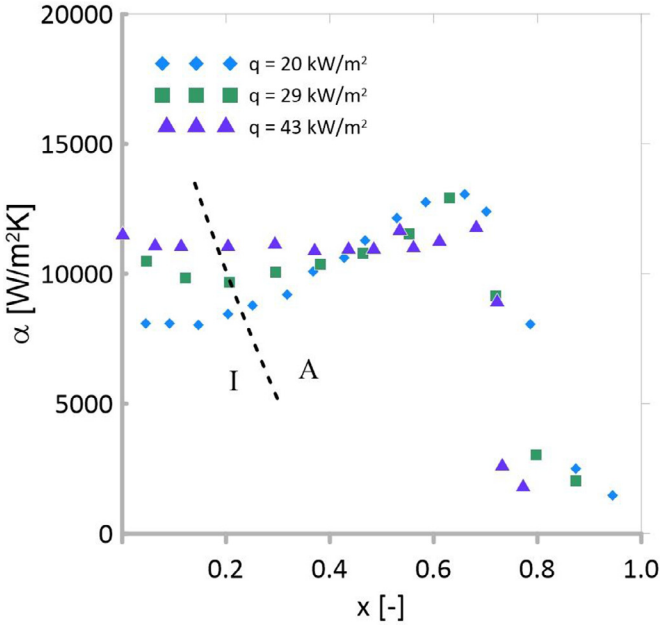

Fig. 14. Heat transfer coefficient in a function of vapor quality for different heat fluxes, reduced pressure p_r=0.4 and mass velocity G = 800 kg/m^{2}s (I – intermittent flow; A – annular flow).

7. Heat transfer

7.1. Effect of heat flux

Figs. 13–15 show the influence of heat flux on overall heat transfer coefficient for different reduced pressures, p_r = 0.2; 0.4 and 0.7 and for one mass velocity (G = 800 kg/m^{2}s). Dashed line presents the boundary between intermittent flow (denoted by letter 'I') and annular flow (denoted by 'A'). The intermittent flow group is represented by bubbly flow, slug flow, and the combination of bubbly and slug flows. For reduced pressure p_r = 0.2, there is no effect of heat flux for the entire vapor quality variation. The

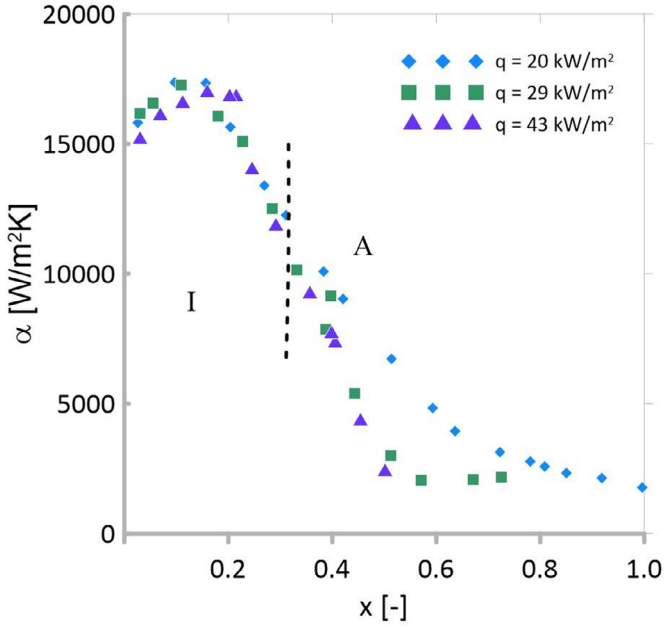

Fig. 15. Heat transfer coefficient in a function of vapor quality for different heat fluxes, reduced pressure p_r=0.7 and mass velocity G = 800 kg/m^{2}s (I – intermittent flow; A – annular flow).

churn flow and annular flow are most common flow structures. Convective boiling is dominant heat transfer mechanism for these conditions. For reduced pressures p_r = 0.3, 0.4, 0.5 the heat transfer increases with increase in the heat flux in the area of low vapor quality whereas with the transition from bubbly flow to annular flow the effect of heat flux diminishes. Both nucleate boiling and convective boiling are present. For reduced pressures p_r = 0.6, 0.7 the heat transfer coefficient is independent of heat flux at the beginning of the evaporation process and decreases with the increase in heat flux for higher values of vapor quality. Such behavior is strongly connected to the occurrence of the dryout phenomena. In our study the occurrence of dryout was identified in two different ways. For decreasing trends we connected it with the drop in heat transfer coefficient higher than 20% across vapor quality increment of 0.1. For other trends we identified dryout by sudden drop in heat transfer coefficient. Similar reasoning was proposed by Marchetto et al. [1]. The higher the reduced pressure the stronger the effect of heat flux on dryout. For the case of reduced pressure p_r = 0.2 the heat flux has no influence on dryout however, for higher values of reduced pressures, we observed that the higher the heat flux the earlier dryout occurs.

7.2. The effect of mass velocity

The effect of mass velocity on heat transfer is presented in Figs. 16–19. Each graph represents different reduced pressures, that is p_r = 0.2; 0.4; 0.6 and 0.7 with fixed heat flux equal to q = 20 kW/m^2. In the case of reduced pressure p_r = 0.2, the heat transfer coefficient increases with mass flux which confirms the dominance of convective boiling. However, at low vapor qualities the heat transfer is independent from mass velocity which indicates influence of nucleate boiling, especially for mass velocity G = 400 kg/m^{2}s. For reduced pressure p_r = 0.4 two trends can be observed, for mass velocities lower than G = 400 kg/m^{2}s the heat transfer coefficient is independent of mass flux whereas for mass velocities higher then G = 400 kg/m^{2}s the heat transfer is independent of mass velocity at the beginning of evaporation process and starts to increase with mass velocity after the transition to an-

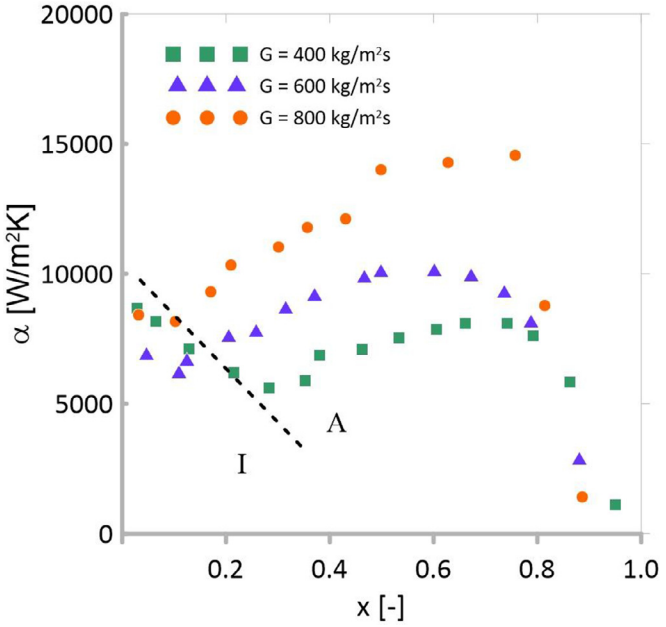

Fig. 16. Heat transfer coefficient in a function of vapor quality for different mass fluxes, reduced pressure p_r=0.2 and heat flux q = 20 kW/m^2 (I – intermittent flow; A – annular flow).

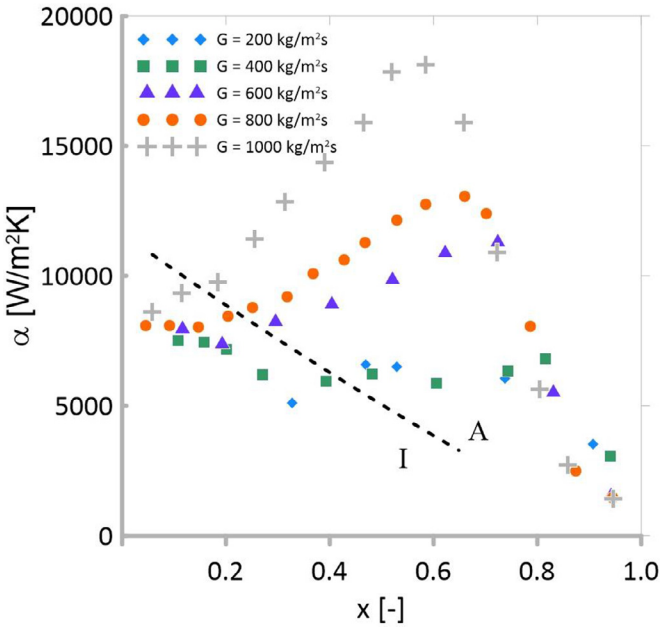

Fig. 17. Heat transfer coefficient in a function of vapor quality for different mass fluxes, reduced pressure p_r=0.4 and heat flux q = 20 kW/m^2 (I – intermittent flow; A – annular flow).

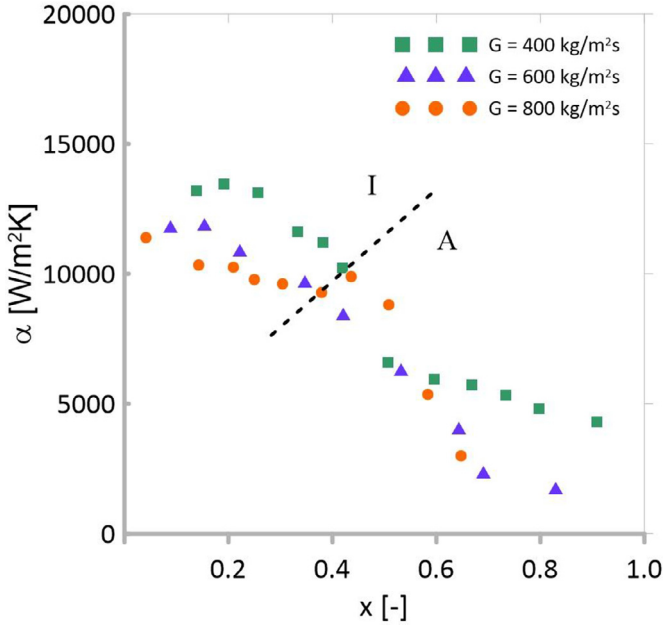

Fig. 18. Heat transfer coefficient in a function of vapor quality for different mass fluxes, reduced pressure p_r=0.6 and heat flux q = 20 kW/m^2 (I – intermittent flow; A – annular flow).

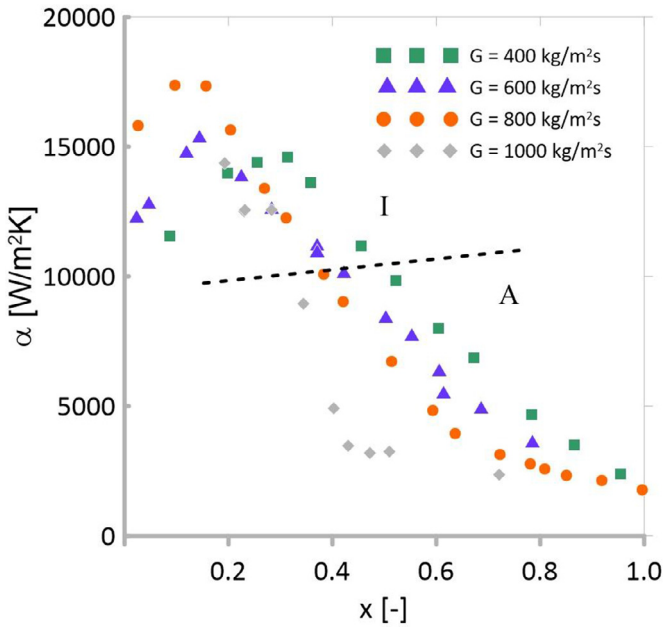

Fig. 19. Heat transfer coefficient in a function of vapor quality for different mass fluxes, reduced pressure p_r=0.7 and heat flux q = 20 kW/m^2 (I – intermittent flow; A – annular flow).

nular flow. For mass fluxes lower than G = 400 kg/m^{2}s the bubbly flow regime was observed even at high values of vapor quality which indicated strong effect of nucleate boiling on overall heat transfer. At the reduced pressures p_r = 0.6, 0.7 the observed trends are entirely different than for the smaller values of reduced pressures. Heat transfer is driven by nucleate boiling only and the heat transfer is independent of mass velocity or even decreases with increase in mass velocity. We assume that the further increase in mass velocity results in decreasing of the liquid film thickness and even complete entrainment of it which leads to deterioration of heat transfer.

7.3. The influence of reduced pressure

One of the most important tasks of this research was to investigate the influence of reduced pressure on overall heat transfer. The results are presented in Figs. 20–22. The results are discussed for different mass fluxes (G = 400, 600, 800 kg/m^{2}s) and the same heat flux (20 kW/m^2). With increase in reduced pressure value the heat transfer increases in the region of low vapor quality. Due to higher values of reduced pressure the nucleation is much more intensive which leads to increase in heat transfer coefficient value. With the increase of vapor quality the effect of reduced pressure diminishes and all of the curves merge, and in

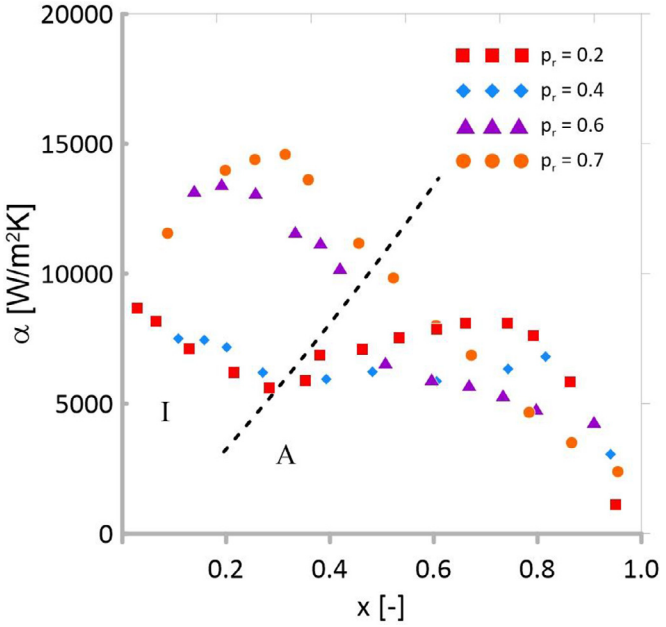

Fig. 20. Heat transfer coefficient in a function of vapor quality for different reduced pressures, mass velocity $G = 400$ kg/m^{2}s and heat flux $q = 20$ kW/m^2 (I – intermittent flow; A – annular flow).

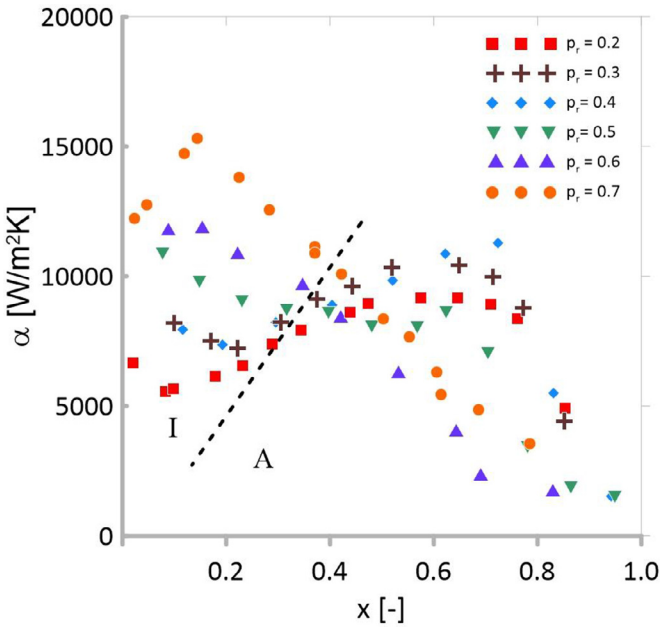

Fig. 21. Heat transfer coefficient in a function of vapor quality for different reduced pressures, mass velocity $G = 600$ kg/m^{2}s and heat flux $q = 20$ kW/m^2 (I – intermittent flow; A – annular flow).

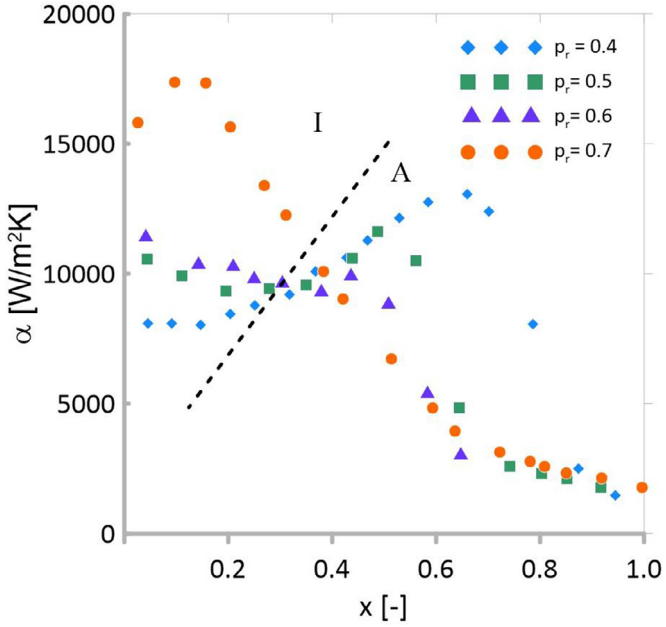

Fig. 22. Heat transfer coefficient in a function of vapor quality for different reduced pressures, mass velocity $G = 800$ kg/m^{2}s and heat flux $q = 20$ kW/m^2 (I – intermittent flow; A – annular flow).

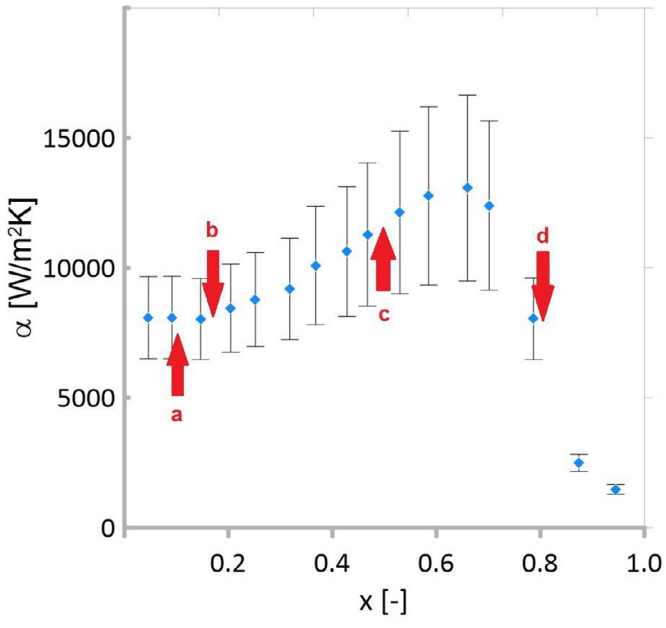

Fig. 23. The heat transfer coefficient in a function of vapor quality. Reduced pressure p_r=0.4, $G = 800$ kg/m^{2}s and $q = 20$ kW/m^2. a) Bubbly flow $x = 0.11$; b) churn flow $x = 0.17$; c) annular flow $x = 0.48$; d) mist flow $x = 0.81$.

the case of reduced pressures $p_r = 0.6, 0.7$ even the decrease in heat transfer can be seen. That behavior can be explained due to decrease of liquid film thickness on the tube wall. Value of reduced pressure has also significant impact on the dryout phenomena. The higher the value of reduced pressure the earlier the dryout occurred which also strongly influences the overall heat transfer. All three heat transfer behaviors described by Marchetto et al. [1] have been observed. Behaviors are strongly influenced by both reduced pressure value and mass velocity. The "no influence" behavior was presented only for reduced pressure equal $p_r = 0.4$ and heat flux equal $q = 43$ kW/m^2 (Fig. 14). Across the experiment the most commonly seen behaviors were decreasing and increasing behaviors with U-shaped trend as the representative of increasing one's. The higher the mass velocity the higher the reduced pressure in which the U-shape trend can be observed. For $G = 400$ kg/m^{2}s the decrease behavior is dominant for most of the reduced pressures with U-shaped trend noticed only for 0.2 reduced pressure. In the case of $G = 600$ kg/m^{2}s U-shaped trend was observed for reduced pressures up to 0.4 and for $G = 800$ kg/m^{2}s up to 0.5.

7.4. The influence of vapor quality and flow structure

Four different trends were found in the terms of vapor quality. The first can be seen for the reduced pressure ranging from

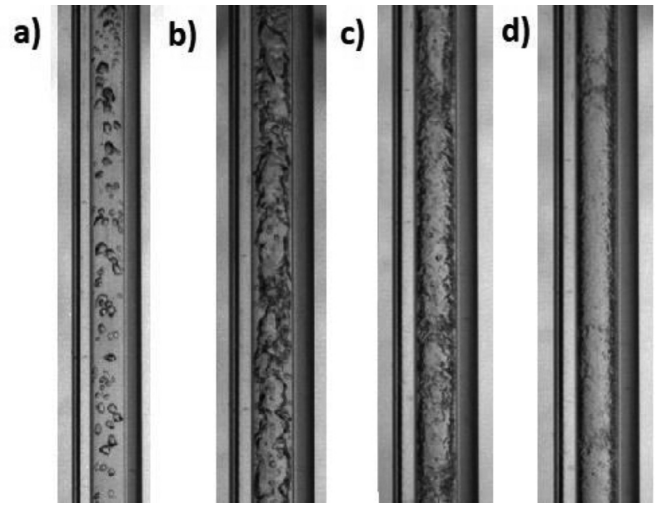

Fig. 24. Visualization of flow patterns during flow boiling. Reduced pressure p_r=0.4, G = 800 kg/m^{2}s and q = 20 kW/m^2. (a) Bubbly flow x = 0.11; (b) churn flow x = 0.17; (c) annular flow x = 0.48; (d) mist flow x = 0.81.

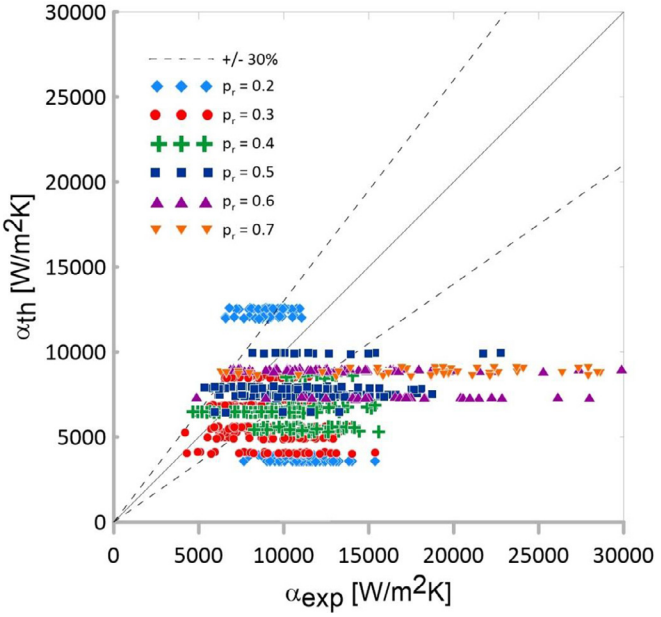

Fig. 25. Results of heat transfer coefficient modeling with a use of a model by Kandlikar and Balasubramanian [18].

p_r=0.2 to 0.5 for mass velocities higher than G = 400 kg/m^{2}s and heat fluxes lower than q = 29 kW/m^2. In this trend the heat transfer coefficient is independent of vapor quality at the beginning of evaporation process and starts to increase for really low values of vapor quality (x < 0.15). The change of the behavior is connected with the transition between bubbly flow and the churn flow, which is presented in Figs. 23 and 24 (point b). In the second trend the heat transfer coefficient initially decreases and after the transition to the annular flow occurs the increase in heat transfer can be seen. Sometimes, especially in the case of really small mass fluxes the heat transfer was independent of vapor quality after the transition to annular flow. These characteristic u- shapes were seen for moderate values of mass velocity and moderate reduced pressures. Observation of these trends suggests that in this specific conditions the flow resembles the flow in conventional channel despite the small diameter of the channel. The third shape noticed was the one in which the heat transfer coefficient is independent of vapor

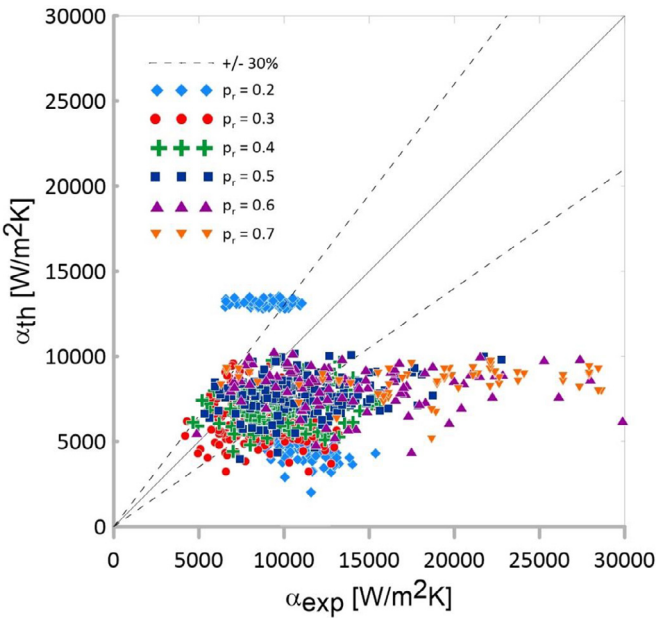

Fig. 26. Results of heat transfer coefficient modeling with a use of a model by Liu and Winterton [19].

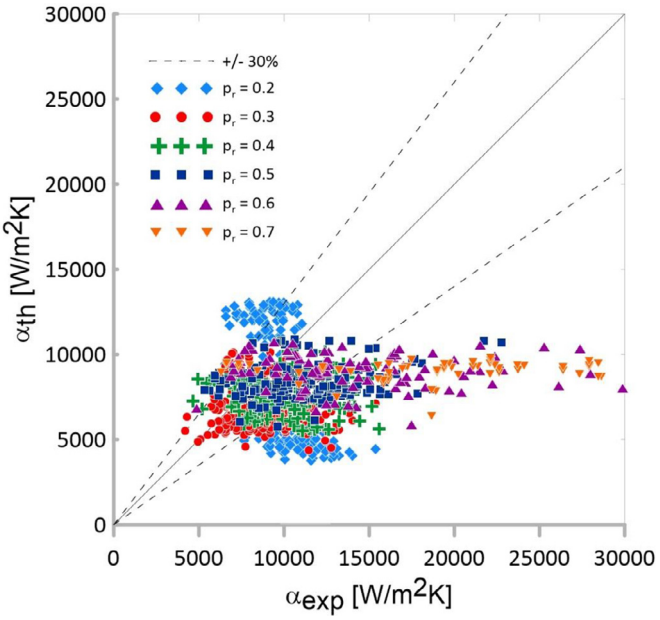

Fig. 27. Results of heat transfer coefficient modeling with a use of the in-house model [20].

quality for the whole vapor quality variation. Such trend was noticed in the case of heat flux equal 43 kW/m^2 and mass velocity equal 800 kg/m^{2}s. The last trend can be seen for reduced pressures 0.6 and 0.7. For these conditions the heat transfer decreases for the whole vapor quality range.

8. Modeling

Figs. 25–28 presents the results of heat transfer coefficient modeling of pre-dryout data with a use of three different models, namely due to Kandlikar and Balasubramanian [18], Liu and Winterton [19] and the in-house model [20]. The highest accuracy was achieved by the in-house model with the mean absolute error equal to 29.31 and 52.22% of data falling within 30% error

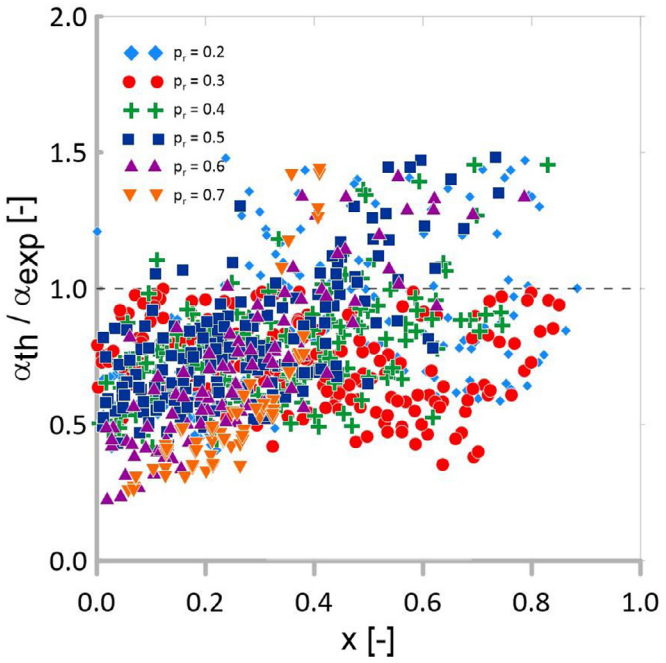

Fig. 28. Results of heat transfer coefficient modeling with a use of the in-house model [20] in a function of vapor quality.

band and 88.20% of data falling within 50% error band. Correlations by Kandlikar and Balasubramanian [18], and Liu and Winterton [19] predicted data with MAE equal 34.87% and 32.42%, respectively. All of the models slightly underestimate the model which can be seen in Fig. 28.

9. Conclusion

Experimental data of heat transfer and pressure drop for R1233zd(E) for moderate to high reduced pressures inside 2 mm circular channel was presented. Influence of heat flux, mass velocity, reduced pressure, vapor quality and flow structures have been discussed.

The pressure drop decreases with reduced pressure and increases with mass velocity. For reduced pressures, $p_r = 0.5$, 0.6, 0.7 the effect of reduced pressure is not noticeable. Heat flux has practically no influence on pressure drop.

At reduced pressures $p_r = 0.2$ and 0.3 heat transfer is driven by convective boiling mostly with nucleate boiling having effect only in the cases of low mass velocities. Heat transfer in this case increases with mass velocity and vapor quality and is independent of heat flux. For reduced pressures $p_r = 0.4$ and $p_r = 0.5$ both nucleate and convective boiling are present, however the nucleate boiling starts to be more dominant here, especially for low mass velocities and high heat fluxes. For lower mass velocities and/or higher heat fluxes the heat transfer decreases or is independent of vapor quality, whereas for higher mass fluxes and/or lower heat fluxes it is initially independent of vapor quality and starts to increase close to the transition from intermittent to annular flow. Overall for these saturation temperatures the heat transfer increases with mass velocity and increases with heat flux. In the case of the reduced pressures $p_r = 0.6$ and 0.7 the two-phase flow resembles the one from conventional channels and the nucleate boiling seems to be a dominant mechanism. Heat transfer coefficient decreases with vapor quality, decreases with mass velocity, and in overall increases or is independent of heat flux. However with the increase of heat flux the dryout occurs much faster which leads to sudden drop in heat transfer capabilities.

All three heat transfer behaviors were observed: no influence, decreasing and increasing behavior Most commonly observed were decreasing behavior and increasing behavior with U-shaped trend as a representative of increasing trends.

The in-house model presented the highest modeling accuracy out of the three tested models, although in the applied form it has not been tested at high reduced pressures. Most of the results are slightly underestimated and improvements concerning higher values of saturation temperature should be considered.

Declaration of Competing Interest

The authors declare that they have no known competing financial interests or personal relationships that could have appeared to influence the work reported in this paper.

CRediT authorship contribution statement

Michał Pysz: Conceptualization, Methodology, Software, Formal analysis, Investigation, Data curation, Writing – original draft, Writing – review & editing, Visualization. **Stanisław Głuch:** Conceptualization, Investigation, Data curation, Writing – original draft. **Dariusz Mikielewicz:** Conceptualization, Methodology, Resources, Writing – review & editing, Supervision, Project administration, Funding acquisition.

Data availability

Data will be made available on request.

Acknowledgments

Work was supported by the National Science Center, Poland [Grant No 2017/25/B/ST8/00755].

References

[1] D.B. Marchetto, D.C. Moreira, R. Revellin, G. Ribatski, A state-of-the-art review on flow boiling at high reduced pressures, Int. J. Heat Mass Transf. 193 (2022) 122951 Sep., doi:10.1016/j.ijheatmasstransfer.2022.122951.
[2] European Social Survey European Research Infrastructure (ESS ERIC)ESS20 - Integrated File, Edition 1.2 [Data Set], Sikt - Norwegian Agency for Shared Services in Education and Research, 2022, doi:10.21338/ESS10E01.
[3] A.V. Belyaev, A.N. Varava, A.V. Dedov, A.T. Komov, An experimental study of flow boiling in minichannels at high reduced pressure, Int. J. Heat Mass Transf. 110 (2017) 360–373 Jul., doi:10.1016/j.ijheatmasstransfer.2017.03.045.
[4] T. Mawatari, H. Mori, An experimental study on characteristics of post-CHF heat transfer in the high subcritical pressure region near to the critical pressure, J. Therm. Sci. Technol. 11 (1) (2016) JTST0006 –JTST0006, doi:10.1299/jtst.2016jtst0006.
[5] R. Charnay, R. Revellin, J. Bonjour, Flow boiling heat transfer in minichannels at high saturation temperatures: part II – assessment of predictive methods and impact of flow regimes, Int. J. Heat Mass Transf. 87 (2015) 653–672 Aug., doi:10.1016/j.ijheatmasstransfer.2015.03.080.
[6] R. Charnay, R. Revellin, J. Bonjour, Flow boiling heat transfer in minichannels at high saturation temperatures: part I – experimental investigation and analysis of the heat transfer mechanisms, Int. J. Heat Mass Transf. 87 (2015) 636–652 Aug., doi:10.1016/j.ijheatmasstransfer.2015.03.081.
[7] R. Charnay, R. Revellin, J. Bonjour, Flow boiling characteristics of R-245fa in a minichannel at medium saturation temperatures, Exp. Therm. Fluid Sci. 59 (2014) 184–194 Nov., doi:10.1016/j.expthermflusci.2014.01.011.
[8] R. Charnay, J. Bonjour, R. Revellin, Experimental investigation of R-245fa flow boiling in minichannels at high saturation temperatures: flow patterns and flow pattern maps, Int. J. Heat Fluid Flow 46 (2014) 1–16 Apr., doi:10.1016/j.ijheatfluidflow.2013.12.002.
[9] M. Billiet, B. Ameel, R. Charnay, R. Revellin, M. de Paepe, Flow regime based heat transfer correlation for R245fa in a 3 mm tube, Int. J. Heat Mass Transf. 117 (2018) 1304–1311 Feb., doi:10.1016/j.ijheatmasstransfer.2017.10.062.
[10] S. Grauso, R. Mastrullo, A.W. Mauro, G.P. Vanoli, Two-phase adiabatic frictional pressure gradients for R410A and CO_2 in a macro channel: experiments and a simplified predictive method for annular flow from low to medium reduced pressures, Exp. Therm. Fluid Sci. 52 (2014) 79–87 Jan., doi:10.1016/j.expthermflusci.2013.08.024.
[11] Y. Zhang, et al., Experimental study of R134a flow boiling in a horizontal tube for evaporator design under typical organic rankine cycle pressures, Int. J. Heat Fluid Flow 71 (2018) 210–219 Jun., doi:10.1016/j.ijheatfluidflow.2018.04.008.

[12] D. del Col, Flow boiling of halogenated refrigerants at high saturation temperature in a horizontal smooth tube, Exp. Therm. Fluid Sci. 34 (2) (2010) 234–245 Feb., doi:10.1016/j.expthermflusci.2009.10.035.
[13] G. Lillo, R. Mastrullo, A.W. Mauro, F. Pelella, L. Viscito, Experimental thermal and hydraulic characterization of R448A and comparison with R404A during flow boiling, Appl. Therm. Eng. 161 (2019) 114146 Oct., doi:10.1016/j.applthermaleng.2019.114146.
[14] Q. Guo, M. Li, X. Tian, Experimental study on flow boiling heat transfer characteristics of R134a, R245fa and R134a/R245fa mixture at high saturation temperatures, Int. J. Therm. Sci. 150 (2020) 106195 Apr., doi:10.1016/j.ijthermalsci.2019.106195.
[15] J.R. Taylor, An Introduction to Error Analysis. The Study of Uncertainties in Physical Measurements, University Science Books, Mill Valley, California, 1997.
[16] V. Gnielinski, New equations for heat and mass transfer in the turbulent flow in pipes and channels, NASA STI Recon Tech. Rep. A 41 (1) (1975) 8–16.
[17] H. Blasius, Das aehnlichkeitsgesetz bei reibungsvorgängen in flüssigkeiten, in: Mitteilungen über Forschungsarbeiten Auf Dem Gebiete des Ingenieurwesens, Springer Berlin Heidelberg, Berlin, Heidelberg, 1913, pp. 1–41, doi:10.1007/978-3-662-02239-9_1.
[18] S.G. Kandlikar, P. Balasubramanian, An extension of the flow boiling correlation to transition, laminar, and deep laminar flows in minichannels and microchannels, Heat Transf. Eng. 25 (3) (2004) 86–93 Apr., doi:10.1080/01457630490280425.
[19] Z. Liu, R.H.S. Winterton, A general correlation for saturated and subcooled flow boiling in tubes and annuli, based on a nucleate pool boiling equation, Int. J. Heat Mass Transf. 34 (11) (1991) 2759–2766 Nov., doi:10.1016/0017-9310(91)90234-6.
[20] D. Mikielewicz, A new method for determination of flow boiling heat transfer coefficient in conventional-diameter channels and minichannels, Heat Transf. Eng. 31 (4) (2010) 276–287 Apr., doi:10.1080/01457630903311694.